Sub-ppb nitrogen dioxide detection with a large linear dynamic range by use of a differential photoacoustic cell and a 3.5 W blue multimode diode laser

Xukun Yin[1, 2], Lei Dong[1, 2,*], Hongpeng Wu[1, 2], Huadan Zheng[1, 2, 3], Weiguang Ma[1, 2], Lei Zhang[1, 2], Wangbao Yin[1, 2], Suotang Jia[1, 2] and Frank K. Tittel[3]

Abstract: A sub-ppb level photoacoustic spectroscopy (PAS)-based sensor for nitrogen dioxide (NO_2) detection was developed by means of a 3.5 W CW multimode diode laser emitting at 447 nm. A differential photoacoustic cell was designed to match the imperfect laser beam and reduce the external acoustic as well as the electromagnetic noise. The diode laser power, gas flow and pressure of the sensor were optimized, which resulted in a NO_2 sensor system with a detection limit of 54 pptv with a 1-s averaging time and an excellent linear dynamic range over > three orders of magnitude. The impact of water vapor as the catalyst on the photoacoustic signal amplitude was also investigated. Continuous measurements covering an eight-day period were performed to demonstrate the stability and robustness of the reported PAS-based NO_2 sensor system.

Keywords: Photoacoustic spectroscopy; Gas sensor; Trace gas detection; High power multimode diode laser; Differential photoacoustic cell

1. Introduction

Environmental pollution has become an extremely serious issue for human health as the result of massive burning of fossil fuels. Nitrogen dioxide (NO_2) is one of the most prevalent air pollutants, which causes photochemical smog and acid rain [1-3]. Ambient NO_2 comes primarily from anthropogenic combustion processes, such as the emissions from cars, power plants and factories. NO_2 is also produced as a result of natural lightning and microbial processes in the soil [1]. The average mixing ratio of NO_2 in the atmosphere is ~ 5-30 part per billion by volume (ppbv), but can be even several orders higher when closer to its sources. Breathing air with a high NO_2 concentration can result in respiratory diseases in humans as well as in animals. According to the US National Ambient Air Quality Standards (NAAQS), the maximum NO_2 concentration in atmospheric air is at a concentration level of 100 ppbv [4]. Therefore, there is a considerable interest in the development of a cost-effective and robust NO_2 sensor system capable of sub-ppb concentration levels and with a large linear dynamic response range for atmospheric monitoring.

Conventional methods for NO_2 measurement include chemiluminescence and wet chemical analysis which are widely employed for atmospheric monitoring. But these methods have a slow response time (*i.e.* minutes-hours) and are non-selective in discriminating between NO and NO_2, especially at low concentrations. Optical methods based on absorption spectroscopy for trace gas detection provide high sensitivity, high selectivity and fast response. Optical methods include infrared tunable diode laser absorption spectroscopy (TDLAS) [5-8], cavity ring down spectroscopy (CRDS) [9-11], cavity enhanced absorption spectroscopy (CEAS) [12] and Faraday rotation spectroscopy (FRS) [13]. Several optical

sensors for NO_2 detection have been demonstrated. For example, M. Langridge *et al.* [14] reported a compact broadband cavity enhanced absorption sensor for NO_2 detection with a sensitivity of 100 pptv for a 60 s data acquisition time. Liu *et al.* [15] reported a FRS based sensor using a widely tunable external cavity quantum cascade laser (EC-QCL) emitting at 6.2 μm as the excitation source, resulting in a sensitivity of ~95 pptv with a 300 s averaging period.

Photoacoustic spectroscopy (PAS) is an important optical method for trace gas detection [16-26]. One of the unique PAS advantages is that its sensitivity is proportional to excitation optical power and thus the performance of PAS-based sensors can benefit from the high output power levels achieved as a result of technology developments by the semiconductor industry. In 2015, H. Zheng *et al.* [27] demonstrated a quartz-enhanced photoacoustic spectroscopy (QEPAS) based NO_2 sensors using a >1 W blue multimode LED emitting at 450 nm. A 1σ detection limit of 1.3 ppbv was achieved with a 1-s integration time. However, an electrical modulation cancellation method (E-MOCAM) had to be employed in order to minimize the noise background from the stray light caused by the poor LED light beam quality and the limited prong spacing (300 μm) of the quartz tuning fork (QTF). This made the sensor system complex. Moreover, the noise background was several orders of magnitude higher than the thermal noise level. Hence, the zero point of the sensor must be recalibrated due to temperature drifts during long term NO_2 concentration measurements.

In 2007, high-power continuous-wave (CW) GaN-based blue diode lasers became commercially available [28]. In 2015, single blue diode lasers capable of several watts optical power were reported [29, 30]. Output power levels of up to 20 W are feasible by means of a

multi-diode laser configuration [31]. NO_2 has a strong visible absorption spectrum at 250-600 nm according to the HITRAN database [32]. Conventional photoacoustic spectroscopy can make the best use of high power diode laser excitation to detect the NO_2, since the QEPAS technique using QTFs is no longer suitable for such high-power diode laser beams due to the limited prong spacing [33, 34]. The conventional photoacoustic cell has a large resonator diameter, which can better match the larger diode laser beam diameter and divergence. In this manuscript, we report on the development of a sub-ppb level NO_2 sensor system using the combination of a differential photoacoustic cell and a 3.5 W blue multimode diode laser.

2. Sensor design

2.1 Selection of high power diode laser

The unresolved NO_2 absorption band between 250 nm-600 nm is depicted in Fig. 1. The visible absorption spectrum of NO_2 is derived from the $^2B_2 \leftarrow {}^2A_1$ and $^2B_1 \leftarrow {}^2A_1$ transition. The vibronic structure of the $^2B_1 \leftarrow {}^2A_1$ transition is regular, while the vibronic structure of the $^2B_2 \leftarrow {}^2A_1$ is complex caused by the low energetic position of the conical intersection between the $\tilde{X}$ and $\tilde{A}$ states of NO_2 [35]. The anomalous vibronic structure of the $^2B_2 \leftarrow {}^2A_1$ transition makes the visible NO_2 absorption band irregular and unresolved.

Furthermore, NO_2 has a photochemical dissociation threshold. When the excitation optical wavelength is < 424 nm, NO_2 photolysis occurs as follows [1]:

$$NO_2 + h\nu \rightarrow NO + O \quad (1)$$

$$O_2 + O + M \rightarrow O_3 + M \quad (2)$$

where M represents N_2 or O_2 or a third molecule. Therefore, the wavelength (λ) selection of the high-power blue diode laser should meet two criteria: 1. λ > 424 nm and 2. λ as close as

possible to the peak area of the NO_2 unresolved absorption band. We selected a 447 nm multimode diode laser with an expected lifetime of 10,000 hours in CW operation (Changchun New Industries Optoelectronics Technology, China, Model MDL-F-447) as the PAS optical excitation source. The temperature of the diode laser was operated at 25°C to stabilize the emitting wavelength. The output optical power of the diode laser is 3.5 W with a driving current of 3 A. The diode laser emission spectrum was obtained using a spectrometer (Avantes, Netherland, Model AVS-DESKTOP-USB2) with a spectral width (FWHM) of ~6 nm, as depicted in Fig. 2 (a). The diode laser emits with a beam divergence $\theta_{\perp}$=26°, $\theta_{\parallel}$=15° due to its multimode characteristics. Hence the diode laser beam with a stripe-like spot was coupled into a multimode quartz optical fiber with a 200 μm core diameter to reshape the diode laser spot into a circular shape. The exit beam was subsequently collimated using an antireflection coated spherical lens with a focal length of 23 mm. The beam divergence was reduced from ~450 mrad behind the fiber facet to 16 mrad behind the collimation lens facet and the diode laser beam diameter is <8 mm within the distance of 15 cm away from the facet of the collimation lens. A photo was taken at 100 mm from the collimator lens to show the reshaped diode laser beam spot size with an output power of 3.2 W, as shown in Fig. 2 (b). The power stability of the laser system was also tested, since the sensitivity is directly proportional to the excitation optical power. The power fluctuations were < 3 % within a 24 hour period.

2.2 Design of a differential photoacoustic cell

A differential photoacoustic cell was designed in order to accommodate and match the beam of the high-power diode laser, as shown in Fig. 3 (a). The differential photoacoustic cell

consists of two identical cylindrical channels performing as two acoustic resonators. The length and diameter of each channel are 90 mm and 8 mm, respectively. The standing acoustic wave can be formed in the acoustic resonator where the excitation diode laser beam is located. Two electret condenser microphones are placed on the walls in the middle of each channel to detect the acoustic pressure. Two 10 mm long buffer volumes were constructed at both ends of the two cylindrical channels to connect the two acoustic resonators and enable them to operate as open-open resonators. The windows are separated from the resonators by the two buffer volumes. The distance between two windows is 110 mm. Such a distance with an 8 mm long resonator diameter allows the collimated beam to pass through easily.

The symmetric double resonator construction of the photoacoustic cell constitutes a differential photoacoustic cell, which resembles the well-known differential Helmholtz resonator [36]. The signals from the two microphones are differentially amplified. As a result, all noise components that are coherent in the two resonators and microphones, such as the flow, window noise and external electromagnetic disturbances are effectively suppressed and thus the signal-to-noise ratio of the reported sensor system is increased. The experimental frequency response of the differential cell is shown in Fig. 3 (b). The resonance frequency of the photoacoustic cell in air was f_0 = 1752.0 Hz and the FWHM of the resonance width was Δf = 70 Hz, resulting in a Q-factor of 25. The cell constant of the differential cell is 10.7 $V/cm^{-1}W$.

3. Experiment setup of sensor system

A schematic of the PAS-based sensor system based on the differential photoacoustic cell and the high-power blue diode laser is depicted in Fig. 4. The diode laser beam was

collimated by use of the collimator described in Section 2.1 and then passed through one of the two acoustic resonators. Two quartz windows with a diameter of 25.4 mm were employed with a transmissivity of >98% at 447 nm. A power meter (Ophir Optronics Solutions. LTD, Israel, Model 3A-ROHS) was placed behind the acoustic resonator to monitor the optical power. A function generator (Agilent, USA, Model 33500B) was employed to generate a square signal with a duty cycle of 50 % and a frequency of f_0, driving the diode laser. This resulted in a mean output power of 1.5 W and 1.3 W in front of and behind the photoacoustic cell due to transmission losses from the windows and the acoustic resonator. The signals from two microphones were amplified by a differential amplifier and then fed into a lock-in amplifier (Stanford Research Systems, USA, Model SR830), which demodulated the signal at 1-f mode. The parameters of a 12 dB/oct filter slope and 1-s time constant were set for the lock-in amplifier, corresponding to a detection bandwidth of Δf = 0.25 Hz. A personal computer was used to acquire and process the signals from both the lock-in amplifier and power meter.

The differential photoacoustic cell has a gas inlet and outlet located on the two buffer volumes. A gas dilution system (Environics Inc., USA, Model EN4000) was used to optimize and assess the performance of the PAS-based sensor system. A 5 ppm NO_2/air calibration gas (Dalian special Gases Co., LTD, China) with an uncertainty of 2% was diluted with zero gas to produce different concentrations by means of the gas dilution system. The sampling system of the PAS-based sensor includes a pressure controller, a needle valve and a diaphragm pump, as shown in Fig. 4. The pressure controller (MKS Instrument Inc., USA, Model 649B) was placed upstream to control and maintain the pressure in the photoacoustic cell, while the

needle valve and the diaphragm pump (KNF Technology Co., LTD, Germany, Model N813.5ANE) were positioned downstream to set the gas flow and provide a pressure difference between the photoacoustic cell and the ambient pressure.

4. Optimization and assessment of sensor performance

4.1 Optimization of power, gas flow rate and pressure

With increasing laser power, saturation may occur, which implies that the depletion from the vibrational excited level slows with respect to the pump rate and no more molecules are able to be excited to higher energy levels with increasing laser power [37-39]. Consequently, the PAS signal will not benefit from further higher laser excitation power. In order to avoid the nonlinear response of the sensor from the complete saturation condition, an experiment to check the saturation level was carried out. The gas flow rate was set to 600 sccm (standard-state cubic centimeter per minute). Zero air was introduced into the acoustic cell. A μV level background signal linearly proportional to the laser power, was observed, as shown in the inset of Fig. 5. The background signal was derived from the stray light due to the multimode nature of high-power laser diodes. Subsequently, a 100 ppbv NO_2/air mixture was fed into the acoustic cell. The signal amplitudes after removing the background signal as a function of the laser power are shown in Fig. 5. With the diode laser power linearly increasing, the growth of the signal amplitudes gradually decreases and a saturation effect occurs, but a complete saturation condition was not reached. Further evaluation tests were implemented with a diode laser mean power of 1.3 W.

The dependence of the signal amplitude and noise on the gas flow rate range from 150 sccm to 700 sccm was investigated with a 100 ppbv NO_2/air mixture as depicted in Fig. 6.

The noise remained constant within this flow rate range, while the signal amplitude increased with a larger flow rate. This behavior can be explained as follows. With an increasing flow rate, unexcited molecules enter the photoacoustic cell. The ratio of the upper state molecules number densities to the total molecules number densities is reduced. As a result the saturation effect decreases and the signal amplitude is enhanced. A gas flow rate of 600 sccm was selected, since with a flow rate of 700 sccm, the signal amplitude barely benefited. The response time of the PAS-based sensor is mainly determined by the exchange rate of the air sample in the acoustic cell and the gas flow system. With a flow rate of 600 sccm and a 1 meters long, 4 mm ID Teflon tube, the exchange rate of air sample is ~3 s.

In PAS, the pressure is a critical parameter, since the *Q*-factor of the acoustic cell, the V-T relaxation rate of target gas and the intensity of the absorption spectrum are pressure dependent. The relationship between the signal amplitude of a 100 ppbv NO_2/air mixture and the pressure are plotted in Fig. 7. The *Q*-factor of the acoustic cell and the intensity of the absorption spectrum increase with gas pressure [40]. Furthermore, collisions between molecules occur more frequently at higher pressure and hence the V-T relaxation rate increases. The combined action of these factors results in a linear increase of the signal amplitude with the total gas pressure as observed in Fig. 7. A gas pressure of 640 Torr was selected as the optimum operating pressure of the PAS-based sensor in order to achieve a PAS signal amplitude as large as possible. This negative pressure allows the sensor system to sample the ambient gas directly.

4.2 Effect of water vapor on the NO_2 signal amplitude

The PAS signal amplitude strongly depends on the V-T relaxation rate of the target gas. Dry NO_2 in nitrogen has a V-T relaxation rate of $\tau < 4$ μs [19]. The resonant frequency of the differential photoacoustic cell is f_0=1752.0 Hz, *i.e.* $1/\omega=1/2\pi f_0 \approx 90$ μs. In case of a fast V-T relaxation rate with respect to the modulation frequency ($\tau << 1/\omega$), the translational gas temperature can follow changes of the laser induced molecular excitation rate [41]. However, water vapor is known to be an efficient catalyst for vibrational energy transfer reactions in the gas phase [42-44]. The typical amount of water vapor in ambient air is 0.5-4%, depending on seasons, climate, weather and topography. Therefore, a detailed analysis of the effect of water vapor on NO_2 signal is essential for precise NO_2 measurements using PAS.

A humidifier (Perma Pure., USA, Model MH-110-24F-4) was used to add water vapor into a mixture of the 100 ppb NO_2/air. The NO_2 signal amplitude was measured at different water concentrations. The results are shown in Fig. 8. With a dry NO_2/air mixture, the signal amplitude is 2.18 mV. A 0.3 % addition of water results in an enhanced signal of 2.5 mV. When the water concentration is >0.3%, the signal amplitude of NO_2 stops increasing and remains constant, since relaxation saturation is reached. Therefore for atmospheric measurements, the effect of water vapor on the NO_2 signal is negligible since the concentration of water vapor is usually >0.3% in the atmosphere.

4.3 Performance assessment of sensor system

To evaluate the performance of the PAS-based sensor for NO_2 detection, the system was operated with optimized parameters that included diode laser power, gas flow rate and pressure. Various NO_2 concentration levels from 50 ppb to 5 ppm were generated with the gas dilution system. Results for the concentration range of 50 ppb to 250 ppb acquired with a 1-s

averaging time (0.25 Hz bandwidth) are plotted in Fig. 9 (a) in order to evaluate the NO_2 sensor detection sensitivity. A constant μV level background signal was observed in zero gas and was removed. Based on the data of the 100 ppbv NO_2/air mixture and an effective absorption cross section of 4.4699×10^{-19} cm^2/molecule [30], the noise equivalent ($1\,\sigma$) concentration is ~ 54 pptv, which corresponds to an absorption coefficient of 1.583×10^{-9} cm^{-1} $W/Hz^{1/2}$ normalized to the detection bandwidth and optical power. To verify the linearity of the PAS-based NO_2 sensor, the concentration values were averaged and plotted in Fig. 9 (b). This plot with linear fitting R square values >0.999 confirms the linearity of the sensor system response to concentration. The linear dynamic range of the PAS based NO_2 sensor covers three orders of magnitude.

5. Continuous monitoring of atmospheric NO_2 concentration levels

The field application of the PAS-based NO_2 sensor with a 1-s averaging time was demonstrated by continuous monitoring of atmospheric NO_2 located in the Shaw Amenities Building on the Shanxi University campus in Taiyuan, China. The gas sampling system acquired air from outdoors. A metal powder sintering filter and a 3 μm micro-pore PTFE filter membrane were used at the front end of the sampling tube as 1st and 2nd stage air filters, respectively, in order to avoid the contamination by dust or soot particles and the interference of aerosols [45, 46].

The NO_2 mixing ratios measured for eight days of continuous monitoring (Oct. 28, 2016 to Nov. 4, 2016) are shown in Fig 10 (a). This time period was selected because winter central heating in Taiyuan starts each year on November 1 and all the heating plants in the Taiyuan area are activated to provide central heating for the city residents. For comparison,

the NO_2 concentration data released by the China National Environmental Monitoring Center (CNEMC) [47] are shown in Fig. 10 (b). This data was acquired by an environmental monitoring station, which is located 7.6 km from our sensor system and uses a chemiluminescence detection method.

The variation trend of the NO_2 concentrations in Fig. 10 (a) is in excellent agreement with Fig. 10 (b). The short duration behavior of concentration fluctuations in Fig. 10 (a) was due to local meteorological conditions, such as wind. In Fig. 10 (b), a similar behavior was not observed due to the fact that the data updating rate was 1 data point/hours, *i.e.* all data within 1 hour was averaged. Furthermore, some details of the concentration variations were observed using our sensor system, as shown in Fig. 10 (a) due to our second level response time of the sensor system. For example, a concentration valley occurred at 4:32 p.m (8:32 a.m. GMT), on Oct. 30, 2016 shown in Fig. 10 (a), but a counterpart is not found in Fig. 10 (b). Before 4 p.m. (8:00 a.m. GMT), on Oct. 31, 2016 the NO_2 concentration maximum is <40 ppbv. Thereafter, the NO_2 concentration steadily increased and the maximum reached up to 80 ppbv during the day due to the presence of the NO_2 sources from the heating plants.

In a previous publication of NO_2 concentration monitoring [15], the NO_2 concentration values in Houston, TX, USA, indicated a periodic variation, since the photolysis process induced by sunlight (see Equations (1) and (2)) and an atmospheric chemistry reaction with ozone (O_3) [1] occurred. The two processes constitute a natural circulation of $NO_2 \rightarrow NO \rightarrow NO_2$. But such a periodic behavior was not observed in Taiyuan, China. Instead, a periodic variation dominated by the NO_2 source was found as shown in Fig. 10. Two periodic peaks of NO_2 concentrations appear at 10:00 a.m. (2:00 a.m. GMT) and 6:00 p.m. (10:00 a.m. GMT)

every day after Nov. 1, 2016. An explanation is that the heating plants are operated continuously in response to high demand at these times.

6. Conclusions

A robust and compact PAS-based sensor system for NO_2 detection was developed. A 3.5 W blue multimode diode laser was used as the excitation source and a differential photoacoustic cell was designed. The combination of a high-power diode laser and differential photoacoustic cell offers advantages, such as high sensitivity, low cost and a large linear dynamic range. The sensitivity of the PAS-based sensor was found to be 54 pptv for NO_2 detection with a 1-s averaging time, which is 24 times lower than an E-MOCAM based QEPAS sensor reported previously [27]. This sensitivity corresponds to a normalized noise equivalent absorption (NNEA) of 1.583×10^{-9} cm^{-1} $W/Hz^{1/2}$. The linear response of this sensor system can cover > 3 orders of magnitude. Continuous monitoring of atmospheric NO_2 for eight days was demonstrated. The agreement between the data released by the CNEMC and ours validated the performance of our sensor system. A further improvement of the PAS based sensor system can be achieved by using a stronger vacuum pump to provide a higher gas flow. In this case, a shorter averaging time can be obtained to improve the sensor response time without sensitivity loss. The reported PAS-based sensor can be employed to measure NO_2 concentration levels for environmental monitoring, atmosphere chemistry research as well as exhaust analysis of motor vehicles as it offers high detection sensitivity and a large linear dynamic range, simultaneously.

Acknowledgements

Lei Dong acknowledges support by National Natural Science Foundation of China (Grant #s. 61622503, 61575113, 61275213) and Open Fund of the State Key Laboratory on Integrated Optoelectronics (IOSKL2015KF25). Frank Tittel acknowledges support by the National Science Foundation (NSF) ERC MIRTHE award and the Robert Welch Foundation (Grant C-0586).

Reference

[1] J. H. Seinfeld, S. N. Pandis, Atmospheric Chemistry and Physics: From air pollution to climate change, John Wiley & Sons, New York, 1998.

[2] A.P. Vasilkov, J. Joiner, L. Oreopoulos, J.F. Gleason, P. Veefkind, E. Bucsela, E.A. Celarier, R.J.D. Spurr, S. Platnick, Impact of tropospheric nitrogen dioxide on the regional radiation budget, Atmospheric Chemistry Physics 9 (2009) 6389–6400.

[3] S. Solomon, W. Portmann, R.W. Sanders, J.S. Daniel, W. Madsen, B. Bartram, E.G. Dutton, On the role of nitrogen dioxide in the absorption of solar radiation, Journal of Geophysical Research 104 (1999) 12047–12058.

[4] United States Environmental Protection Agency Website. http://www.epa.gov.

[5] C. G. Li, L. Dong, C.T. Zheng, F. K. Tittel, Compact TDLAS based optical sensor for ppb-level ethane detection by use of a 3.34 μm room-temperature CW interband cascade laser, Sensors and Actuators B: Chemical 232 (2016) 188-194.

[6] L. Dong, F. K. Tittel, C. G. Li, N. P. Sanchez, H. P. Wu, C. T. Zheng, Y. J. Yu, A. Sampaolo, R. J. Griffin, Compact TDLAS based sensor design using interband cascade

lasers for mid-IR trace gas sensing, Optics Express 24 (2016) A528-A535.

[7] L. Dong, C. G. Li, N. P. Sanchez, A. K. Gluszek, R. J. Griffin, F. K. Tittel, Compact CH_4 sensor system based on a continuous-wave, low power consumption, room temperature interband cascade laser, Applied Physics Letters 108 (2016) 011106.

[8] A. Karpf, G. N. Rao, Absorption and wavelength modulation spectroscopy of NO_2 using a tunable, external cavity continuous wave quantum cascade laser, Applied Optics 48 (2009) 408-413.

[9] P. Ehlers, I. Silander, J. Wang, A. Foltynowicz, O. Axner, Fiber-laser-based noise-immune cavity-enhanced optical heterodyne molecular spectrometry incorporating an optical circulator, Optics Letters 39 (2014) 279-282.

[10] Z. X. Li, W. G. Ma, X. F. Fu, W. Tan, G. Zhao, L. Dong, L. Zhang, W. B. Yin, S. T. Jia, Continuous-wave cavity ringdown spectroscopy based on the control of cavity reflection, Optics Express 21 (2013) 17961-17971.

[11] H. Fuchs, W. P. Dubé, B. M. Lerner, N. L. Wagner, E. J. Williams, S. S. Brown, A sensitive and versatile detector for atmospheric NO_2 and NOx based on blue diode laser cavity ring-down spectroscopy, Environmental Science & Technology 43 (2009) 7831-7836.

[12] T. Wu, W. Zhao, W. D. Chen, W. Zhang, X. M. Gao, Incoherent broadband cavity enhanced absorption spectroscopy for in situ measurements of NO_2 with a blue light emitting diode, Applied Physics B 94 (2009) 85-94.

[13] R. Lewicki, J. H. Doty III, R. F. Curl, F. K. Tittel, G. Wysocki, Ultrasensitive detection of nitric oxide at 5.33 μm by using external cavity quantum cascade laser-based Faraday

rotation spectroscopy, Proceedings of the National Academy of Sciences of the United States of America 106 (2009) 12587-12592.

[14] J. M. Langridge, S. M. Ball, R. L. Jones, A compact broadband cavity enhanced absorption spectrometer for detection of atmospheric NO_2 using light emitting diodes, Analyst 131 (2006) 916-922.

[15] K. Liu, R. Lewickic, F. K. Tittel, Development of a mid-infrared nitrogen dioxide sensor based on Faraday rotation spectroscopy, Sensors and Actuators B: Chemical 237 (2016) 887-893.

[16] J. P. Waclawek, H. Moser, B. Lendl, Compact quantum cascade laser based quartz enhanced photoacoustic spectroscopy sensor system for detection of carbon disulfide, Optics Express 24 (2016) 6559-6571.

[17] H. M. Yi, K. Liu, W. D. Chen, T. Tan, L. Wang, X. M. Gao, Application of a broadband blue laser diode to trace NO_2 detection using off-beam quartz enhanced photoacoustic spectroscopy, Optics Letters 36 (2011) 481-483.

[18] J. P. Lima, H. Vargas, A. Miklos, M. Angelmahr, P. Hess, Photoacoustic detection of NO_2 and N_2O using quantum cascade lasers, Applied Physics B 85 (2006) 279-284.

[19] J. Kalkman, H. W. Van Kesteren, Relaxation effects and high sensitivity photoacoustic detection of NO_2 with a blue laser diode, Applied Physics B 90 (2008) 197-200.

[20] H. D. Zheng, L. Dong, Y. Ma, H. P. Wu, X. L. Liu, X. K. Yin, L. Zhang, W. G. Ma, W. B. Yin, L. T. Xiao, S. T. Jia, Scattered light modulation cancellation method for sub-ppb-level NO_2 detection in a LD-excited QEPAS system, Optics Express 24 (2016) A752-A761.

[21] Y. Cao, W. Jin, H. L. Ho, Optimization of spectrophone performance for quartz-enhanced photoacoustic spectroscopy, Sensors and Actuators B: Chemical 174 (2012) 24-30.

[22] S. Böttger, M. Köhring, U. Willer, W. Schade, Off-beam quartz-enhanced photoacoustic spectroscopy with LEDs, Applied Physics B 113 (2013) 227-232.

[23] Y. F. Ma, Y. He, X. Yu, C. Chen, R. Sun, F. K. Tittel, HCl ppb-level detection based on QEPAS sensor using a low resonance frequency quartz tuning fork, Sensors and Actuators B-Chemical 233 (2016) 388-393.

[24] H. P. Wu, L. Dong, W. Ren, W. B. Yin, W. G. Ma, L. Zhang, S. T. Jia, F. K. Tittel, Position effects of acoustic micro-resonator in quartz enhanced photoacoustic spectroscopy, Sensors and Actuators B: Chemical 206 (2015) 364-370.

[25] M. Pushkarsky, A. Tsekoun, I. G. Dunayevskiy, R. Go, C. K. N. Patel, Sub-parts-per-billion level detection of NO_2 using room-temperature quantum cascade lasers, Proceedings of the National Academy of Sciences of the United States of America 103 (2006) 10846-10849.

[26] L. Dong, H. P. Wu, H. D. Zheng, Y. Y. Liu, X. L. Liu, W. Z. Jiang, L. Zhang, W. G. Ma, W. Ren, W. B. Yin, S. T. Jia, F. K. Tittel, Double acoustic microresonator quartz-enhanced photoacoustic spectroscopy, Optics Letters 39 (2014) 2479-2482.

[27] H. D. Zheng, L. Dong, X. K. Yin, X. L. Liu, H. P. Wu, L. Zhang, W. G. Ma, W. B. Yin, S. T. Jia, Ppb-level QEPAS NO_2 sensor by use of electrical modulation cancellation method with a high power blue LED, Sensors and Actuators B-Chemical, 208 (2015) 173-179.

[28] T. Kozaki, S. Nagahama, T. Mukai, Recent progress of high-power GaN-based laser diodes, Proceedings of the SPIE 6485 (2007) 648503

[29] A. Pourhashemi, R. M. Farrell, D. A. Cohen, D. L. Becerra, S. P. DenBaars, S. Nakamura, CW operation of high-power blue laser diodes with polished facets on semi-polar $(20\bar{2}\bar{1})$ GaN substrates, Electronics Letters 52 (2016) 2003-2005.

[30] A. Pourhashemi, R. M. Farrell, D. A. Cohen, J. S. Speck, S. P. DenBaars, S. Nakamura, High-power blue laser diodes with indium tin oxide cladding on semipolar $(20\bar{2}\bar{1})$ GaN substrates, Applied Physics Letters 106 (2015) 111105

[31] Changchun New Industries Optoelectronics Technology http://www.cnilaser.com.

[32] The HITRAN database http://www.hitran.com.

[33] H. P. Wu, L. Dong, H. D. Zheng, X. L. Liu, X. K. Yin, W. G. Ma, L. Zhang, W. B. Yin, S. T. Jia, F. K. Tittel, Enhanced near-infrared QEPAS sensor for sub-ppm level H_2S detection by means of a fiber amplified 1582 nm DFB laser, Sensors and Actuators B-Chemical 221 (2015) 666-672.

[34] H. P. Wu, A. Sampaolo, L. Dong, P. Patmisco, X. L. Liu, H. D. Zheng, X. K. Yin, W. G. Ma, L. Zhang, W. B. Yin, V. Spagnolo, S. T. Jia, F. K. Tittel, Quartz enhanced photoacoustic H_2S gas sensor based on a fiber-amplifier source and a custom tuning fork with large prong spacing, Applied Physics Letters 107 (2015) 111104.

[35] E. Haller, H. Köppel, L. S. Cederbaum, The visible absorption spectrum of NO_2: a three-mode nuclear dynamics investigation, Journal of molecular spectroscopy 111 (1985) 377-397.

[36] A. Miklos, P. Hess, Z. Bozoki, Application of acoustic resonators in photoacoustic trace gas analysis and metrology, Review of Scientific Instruments 72 (2001) 1937-1955.

[37] C. Y. Yuan, Z. X. Yan, G. Meng, Z. H. Li, L. P. Shang, Photoacoustic signal saturation

characteristics of concentrated gases, Acta Physica Sinica 59 (2010) 6908-6913.

[38] F. J. M. Harren, F. G. C. Bijnen, J. Reuss, L. A. C. J. Voesenek, C. W. P. M. Blom, Sensitive intracavity photoacoustic measurements with a CO_2 waveguide laser, Applied Physics B 50 (1990) 137-144.

[39] D. C. Dumitras, D. C. Dutu, C. Matei, A. M. Magureanu, M. Petrus and C. Popa, Laser photoacoustic spectroscopy: principles, instrumentation, and characterization, Journal of Optoelectronics and Advanced Materials 9 (2007) 3655–3701.

[40] L. Dong, A. A. Kosterev, D. Thomazy, F. K. Tittel, QEPAS spectrophones: design, optimization, and performance, Applied Physics B 100 (2010) 627-635.

[41] G. Wysocki, A. A. Kosterev, F. K. Tittel, Influence of molecular relaxation dynamics on quartz-enhanced photoacoustic detection of CO_2 at λ = 2 μm, Applied Physics B 85 (2006) 301-306.

[42] X. K. Yin, L. Dong, H. D. Zheng, X. L. Liu, H. P. Wu, Y. F. Yang, W. G. Ma, L. Zhang, W. B. Yin, L. T. Xiao, S. T. Jia, Impact of humidity on quartz-enhanced photoacoustic spectroscopy based CO detection using a near-IR telecommunication diode laser, Sensors 16 (2016) 162.

[43] A. A. Kosterev, T. S. Mosely, F. K. Tittel, Impact of humidity on quartz-enhanced photoacoustic spectroscopy based detection of HCN, Applied Physics B 85 (2006) 295-300.

[44] A. Veres, Z. Bozóki, Á. Mohácsi, M. Szakáll, G. Szabó, External cavity diode laser based photoacoustic detection of CO_2 at 1.43 micron: the effect of molecular relaxation, Applied spectroscopy 57 (2003) 900-905.

[45] W. X. Zhao, M. Dong, W. D. Chen, X. J. Gu, C. J. Hu, X. M. Gao, W. Huang, W. J. Zhang, Wavelength-resolved optical extinction measurements of aerosols using broad-band cavity-enhanced absorption spectroscopy over the spectral range of 445–480 nm, Analytical Chemistry 65 (2013) 2260-2268.

[46] D. A. Lack, M. S. Richardson, D. Law, J. M. Langridge, C. D. Cappa, R. J. McLaughlin, D. M. Murphy, Aircraft instrument for comprehensive characterization of aerosol optical properties, part 2: black and brown carbon absorption and absorption enhancement measured with photo acoustic spectroscopy, Aerosol Science and Technology 46 (2012) 555-568.

[47] China National Environmental Monitoring Center http://www.cnemc.cn/.

Figure captions

Fig. 1 NO_2 unresolved absorption band between 250 nm - 600 nm and a photochemical dissociation threshold: $\lambda < 424$ nm.

Fig. 2 (a) Emission spectrum of the high-power CW laser diode; **(b)** Laser diode beam spot with an output power of 3.2 W after being reshaped by an optical fiber and collimator.

Fig. 3 (a) Schematic of the differential photoacoustic cell; **(b)** Frequency response of the differential photoacoustic cell.

Fig. 4 Schematic of the PAS-based sensor system based on a differential photoacoustic cell and a high power blue diode laser.

Fig. 5 Signal amplitudes after removing the background signal as a function of the laser average power. Inset: μV level background signal linear dependence on the diode laser power. Data was acquired with a 100 ppbv NO_2/air mixture.

Fig. 6 Dependence of the signal amplitude and noise for a 100 ppbv NO_2/air mixture on the gas flow rate.

Fig. 7 Relationship between the signal amplitude of a 100 ppbv NO_2/air mixture and the gas pressure inside the differential photoacoustic cell.

Fig. 8 NO_2 signal amplitude for a 100 ppbv NO_2/air mixture as a function of different H_2O concentrations

Fig. 9 (a) PAS-based sensor signals at five NO_2 concentration levels. **(b)** Linearity of the PAS-based NO_2 sensor system.

Fig. 10 (a) NO_2 concentrations measured during an 8 day period in Nov. 2016 on the Shanxi University campus, Taiyuan, China. Before winter central heating in Taiyuan; After winter

central heating in Taiyuan. (b) Corresponding data available from a nearby Chinese National Environmental Monitoring Centre.

Fig.1.

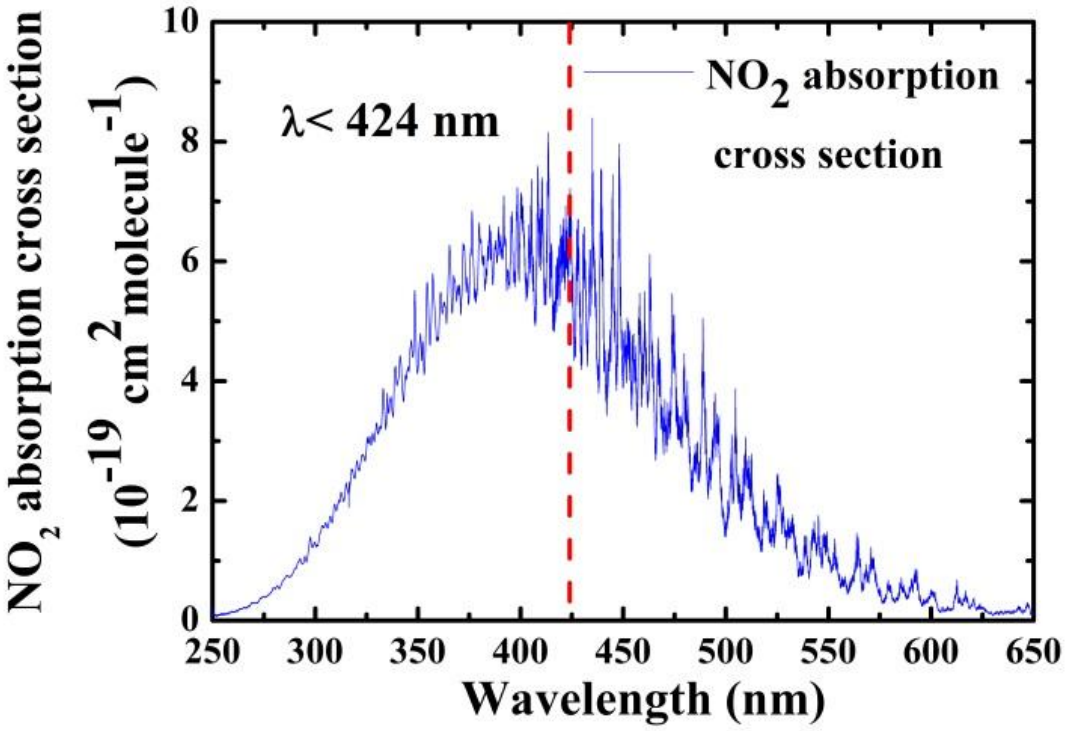
NO2 absorption cross section
(10-19 cm2molecule-1)
λ< 424 nm
NO2 absorption
cross section
Wavelength (nm)
0
2
4
6
8
10
250
300
350
400
450
500
550
600
650

Fig.2 (a).

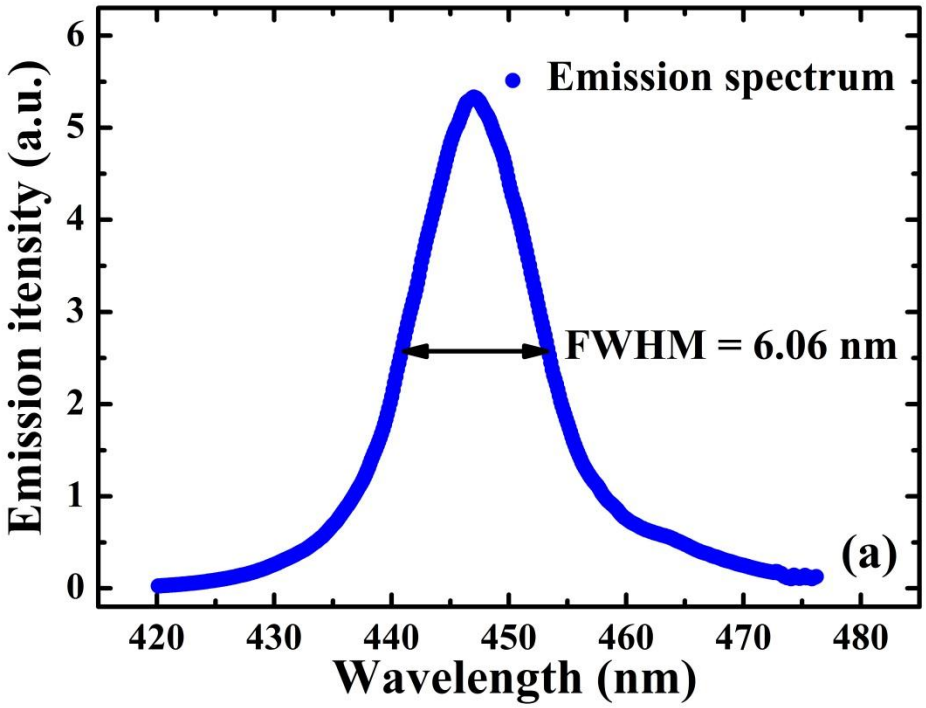
Emission spectrum
FWHM = 6.06 nm
(a)
Emission itensity (a.u.)
Wavelength (nm)
0
1
2
3
4
5
6
420
430
440
450
460
470
480

Fig.2 (b)

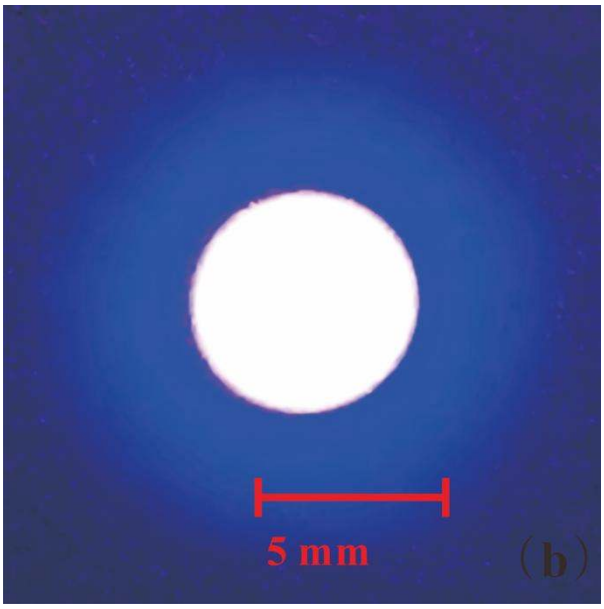

Fig.3 (a)

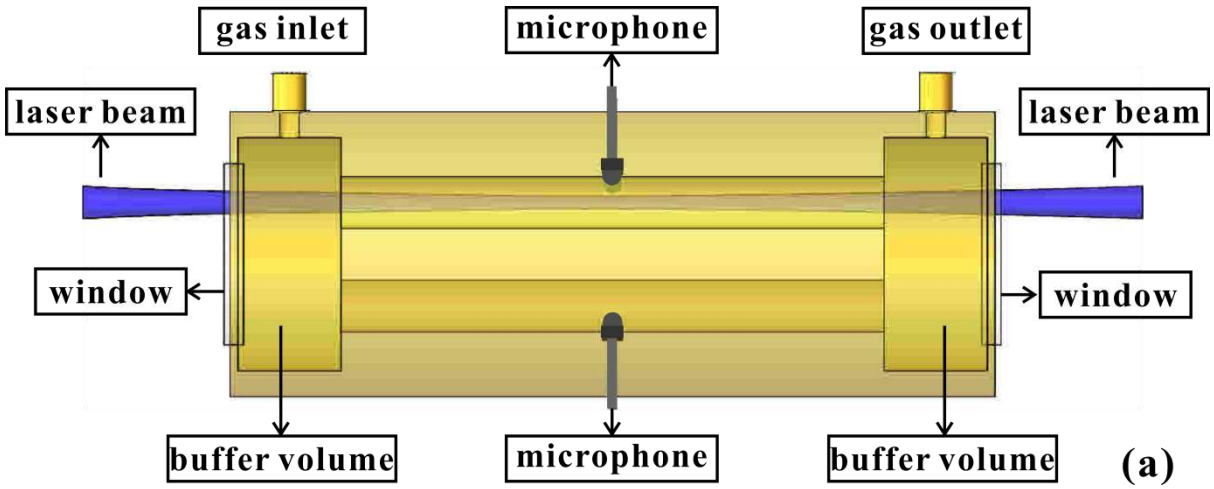
gas inlet
microphone
gas outlet
laser beam
laser beam
window
window
buffer volume
microphone
buffer volume
(a)

Fig.3 (b)

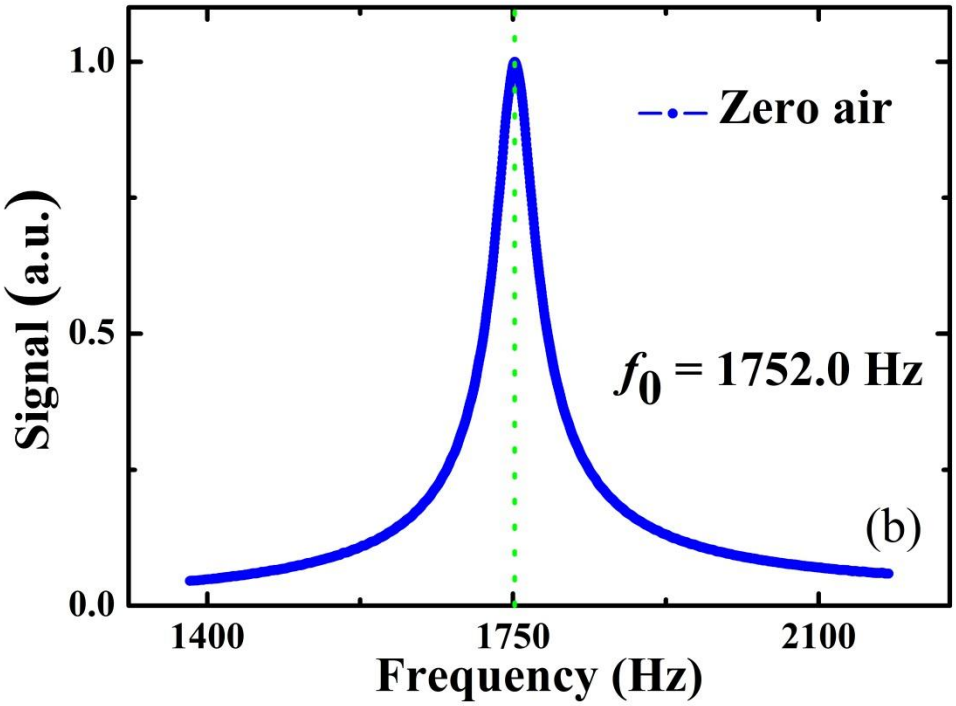
1.0
0.5
0.0
Signal (a.u.)
1400
1750
2100
Frequency (Hz)
Zero air
f_0 = 1752.0 Hz
(b)

Fig.4

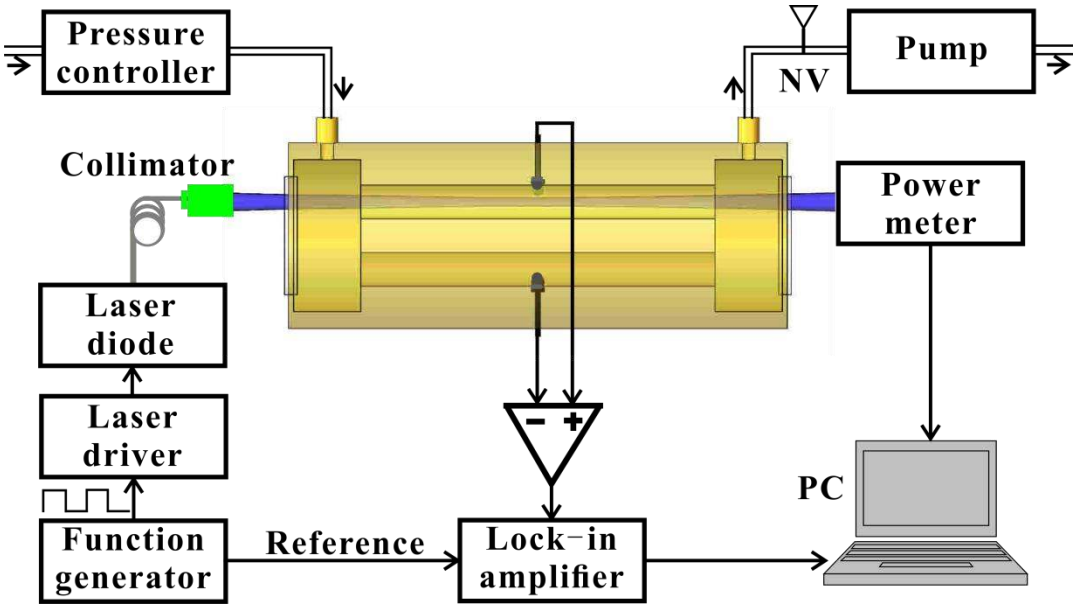
Pressure controller
Pump
NV
Collimator
Power meter
Laser diode
Laser driver
PC
Function generator
Reference
Lock-in amplifier

Fig.5

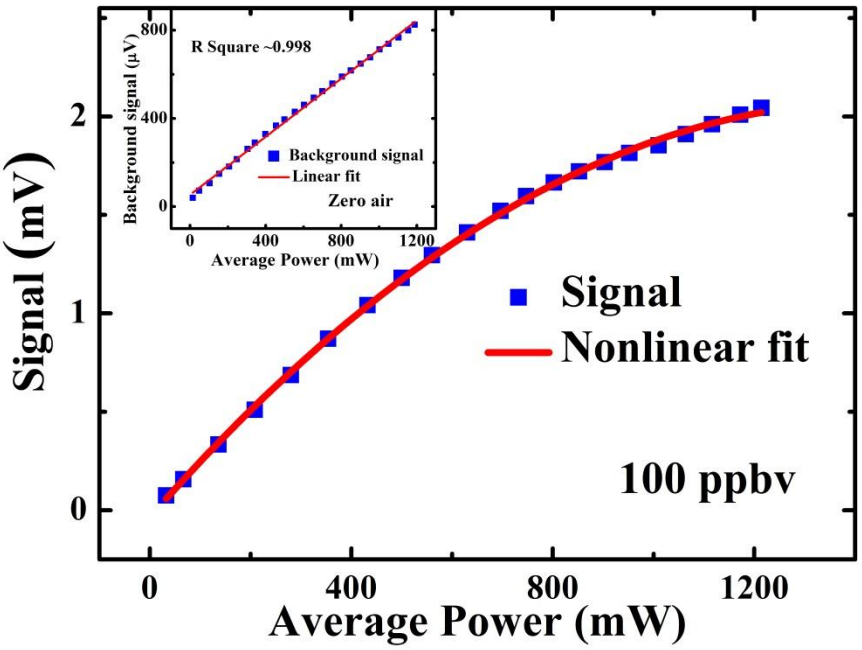
Signal (mV)
Average Power (mW)
Signal
Nonlinear fit
100 ppbv
R Square ~0.998
Background signal (μV)
Background signal
Linear fit
Zero air
Average Power (mW)

Fig.6

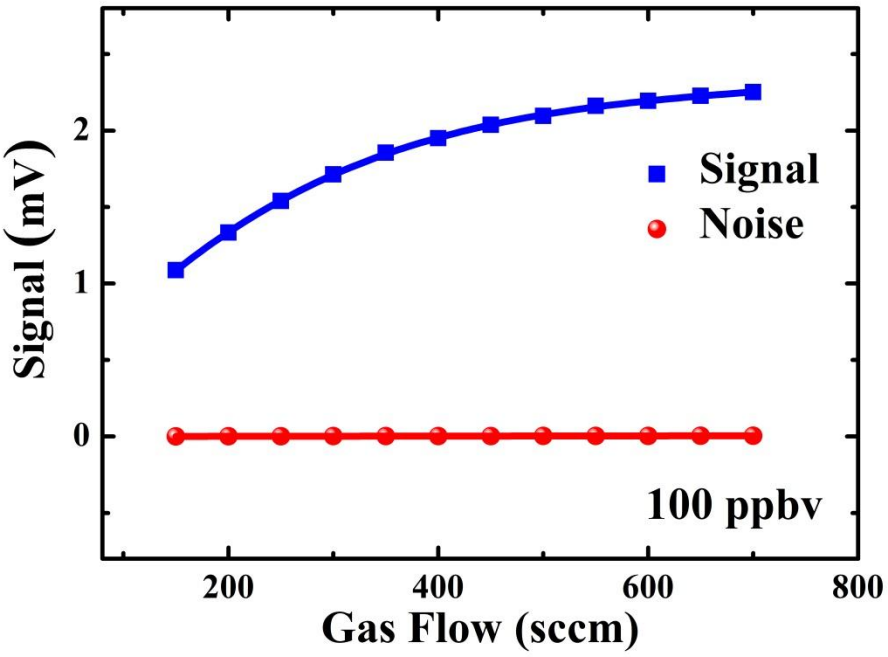
Signal (mV)
2
1
0
Signal
Noise
100 ppbv
200
400
600
800
Gas Flow (sccm)

Fig.7

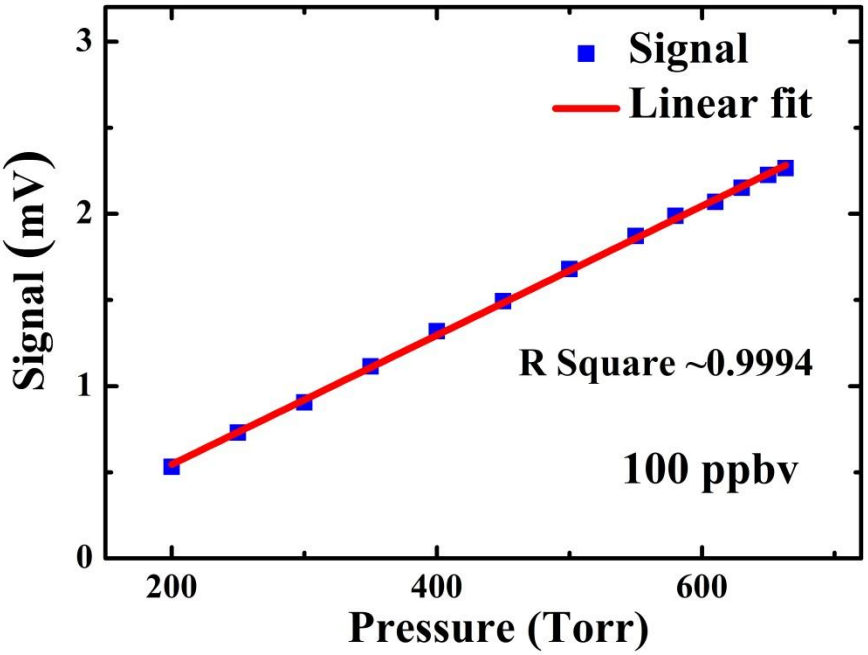
Signal
Linear fit
R Square ~0.9994
100 ppbv
Signal (mV)
Pressure (Torr)
0
1
2
3
200
400
600

Fig.8

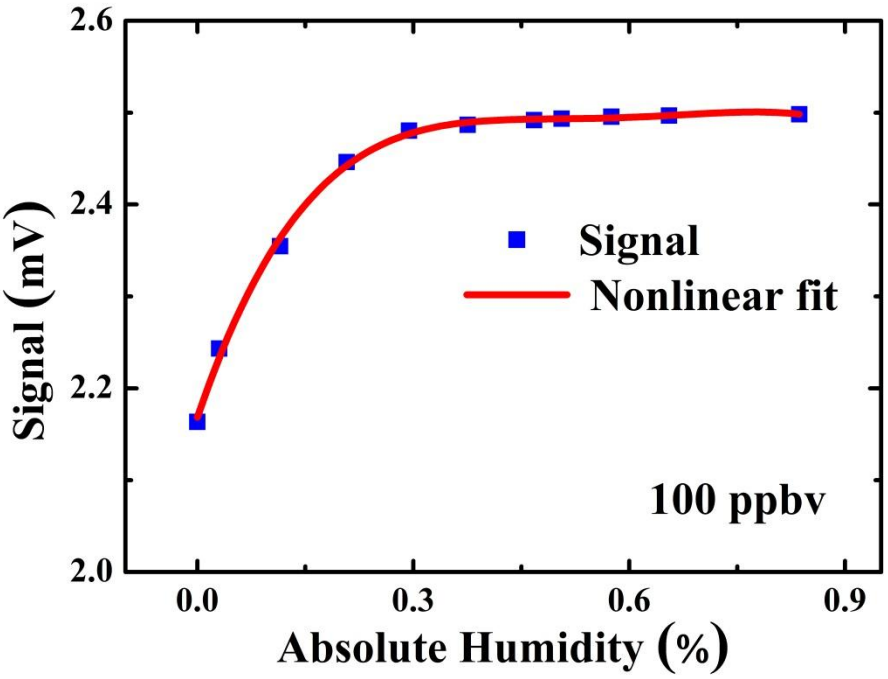
2.6
2.4
2.2
2.0
Signal (mV)
0.0
0.3
0.6
0.9
Absolute Humidity (%)
Signal
Nonlinear fit
100 ppbv

Fig.9 (a)

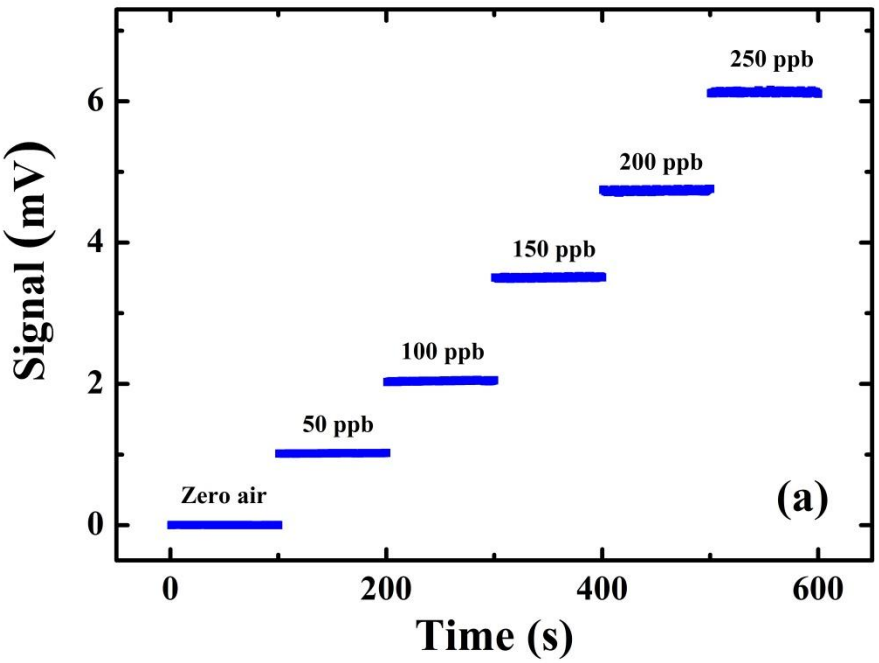
Signal (mV)
Time (s)
0
2
4
6
0
200
400
600
Zero air
50 ppb
100 ppb
150 ppb
200 ppb
250 ppb
(a)

Fig.9 (b)

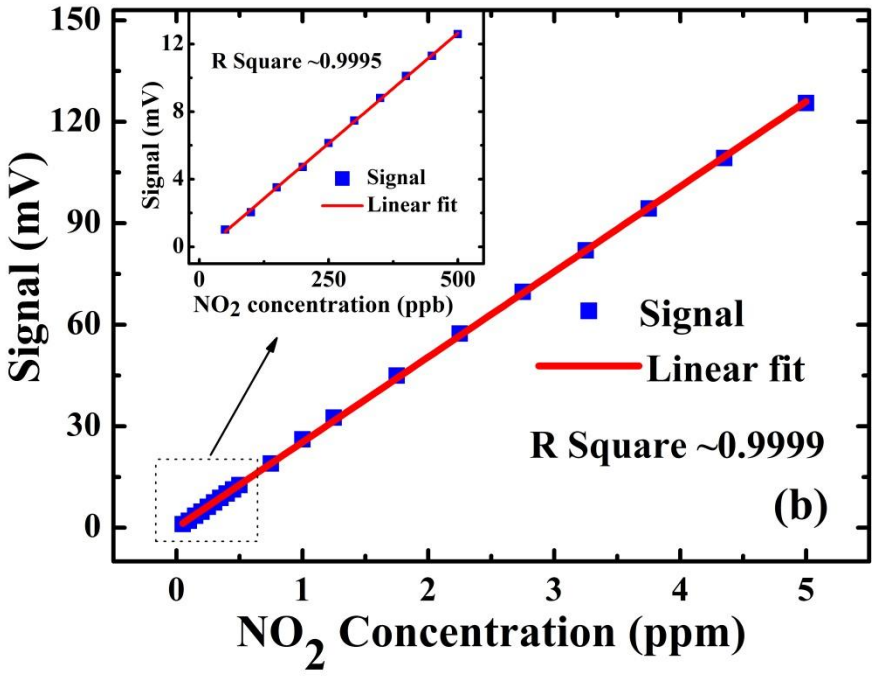
Signal (mV)
NO2 Concentration (ppm)
Signal
Linear fit
R Square ~0.9999
(b)
R Square ~0.9995
Signal (mV)
NO2 concentration (ppb)
Signal
Linear fit

Fig.10

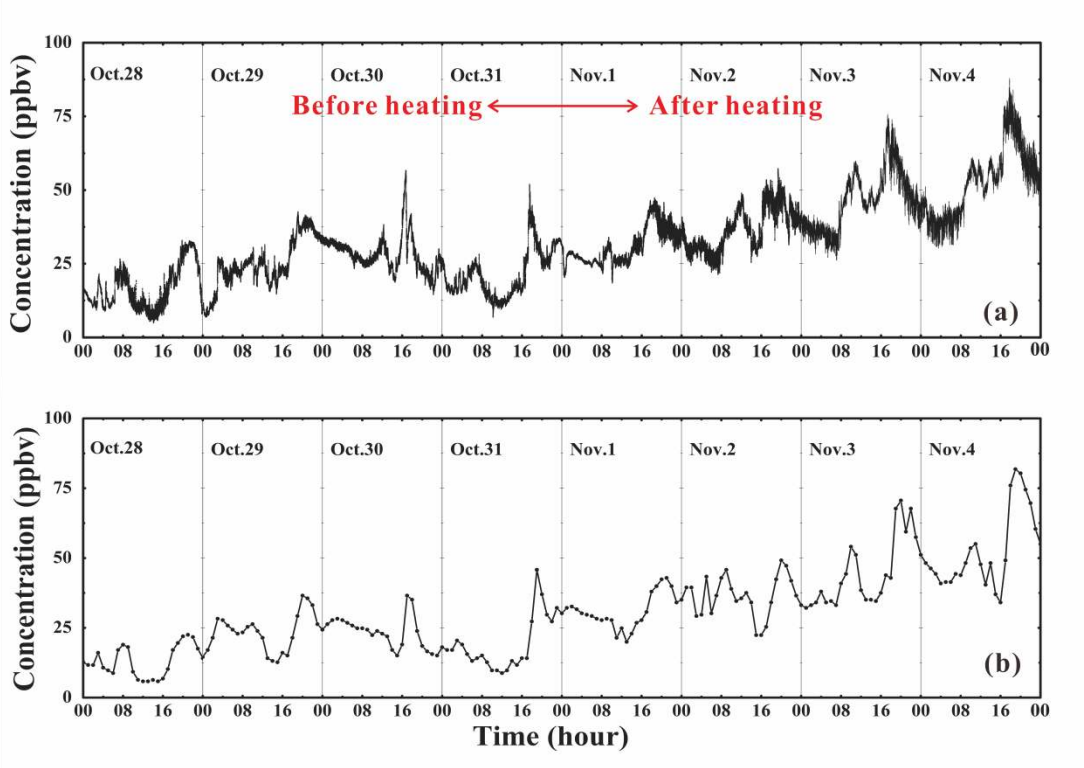
Concentration (ppbv)
100
75
50
25
0
Oct.28
Oct.29
Oct.30
Oct.31
Nov.1
Nov.2
Nov.3
Nov.4
Before heating
After heating
(a)
(b)
00 08 16 00 08 16 00 08 16 00 08 16 00 08 16 00 08 16 00 08 16 00 08 16 00
Time (hour)